# SYNTHESIS OF THERMO-MAGNETO-RESPONSIVE POLY(*N*-ISOPROPYLACRYLAMIDE)-BASED COMPOSITE HYDROGELS FOR ADSORPTION-DESORPTION OF CHROMIUM (III) IONS

**by**

**CHEN JIAN JIE**

**Thesis submitted in fulfilment of the requirements for the degree of Doctor of Philosophy**

**July 2019**

## ACKNOWLEDGEMENT

First of all, with earnest gratefulness and appreciation, I would like to express my deepest gratitude to my parents and my family members for their support, tolerance and encouragement. They have provided me with great confidence to face the obstacles throughout my entire study. My sincere thanks to my dedicated supervisors, Assoc. Prof. Dr. Ooi Boon Seng, Prof. Lim Jit Kang and Prof. Dr. Abdul Latif Ahmad for their excellent supervision and enormous patience throughout my entire PhD study. I would like to thank them for their keen observations on my research works and their valuable suggestions on the areas that required further study. Thank you very much for the delicate help and invaluable advice throughout my entire study.

Furthermore, I would also like to express my gratitude to School of Chemical Engineering, USM who offers the great opportunity to me for gaining a lot of valuable knowledge from the research and thesis. Not forgetting to thank administrative staffs, office staffs and technicians for giving me full support throughout my research works. In addition, I would like to express my heartfelt gratitude and thank to all my beloved friends and colleagues for rendering their help, kindness and moral support on me. I might not be able to achieve what I want to be without their support.

Last but not least, the financial supports from Universiti Sains Malaysia Research University Grant (RUI) (1001/PJKIMIA/8014012), Ministry of Energy, Science, Technology, Environment and Climate Change Malaysia (DANA (R&D) MESTECC) (305/PJKIMIA/6013701) and Ministry of Higher Education (MyPhD) are gratefully acknowledged.

***Chen Jian Jie***

***March 2019***

## TABLE OF CONTENTS


| | Page |
|---|---|
| **ACKNOWLEDGEMENT** | ii |
| **TABLE OF CONTENTS** | iii |
| **LIST OF TABLES** | x |
| **LIST OF FIGURES** | xi |
| **LIST OF ABBREVIATIONS** | xviii |
| **LIST OF SYMBOLS** | xxiii |
| **ABSTRAK** | xxv |
| **ABSTRACT** | xxvii |

**CHAPTER ONE: INTRODUCTION**

| | | |
|---|---|---|
| 1.1 | Research Overview | 1 |
| 1.2 | Thermo-responsive Composite Hydrogels for Heavy Metal Removal | 2 |
| 1.3 | Polydispersity and Undesired Aggregation of Composite Hydrogels | 5 |
| 1.4 | Release of Metal Ions and Regeneration of the Composite Hydrogels | 6 |
| 1.5 | Chromium and Its Interaction with PNIPAM | 7 |
| 1.6 | Problem Statement | 9 |
| 1.7 | Research Objectives | 12 |
| 1.8 | Scopes of Study | 13 |
| 1.9 | Organization of the Thesis | 16 |

**CHAPTER TWO: LITERATURE REVIEW**


2.1 Stimuli-responsive Polymeric Hydrogels 19

2.1.1 Thermo-responsive Hydrogels 21

2.1.2 pH-responsive Hydrogels 25

2.1.3 Photo-responsive Hydrogels 25

2.2 Iron Oxides Magnetic Nanoparticles (MNPs) as Cores for Hydrogels 26

2.3 Architectural Designs of PNIPAM-based Hydrogel-MNPs Composites 27

2.3.1 PNIPAM-MNPs Core-Shell Structures 27

2.3.2 Incorporation of MNPs within PNIPAM-matrix 31

2.4 Synergistic Behaviour of Thermo-magneto-responsiveness of the PNIPAM-encapsulated MNPs Composite Hydrogels. 35

2.5 Polymeric Matrix for Metal Ions Removal 38

2.5.1 Biopolymer for Metal Ions Removal 41

2.5.2 Synthetic Polymeric Hydrogels for Metal Ions Removal 45

2.6 Regeneration of Metal-loaded PNIPAM Hydrogel via Thermal Actuation 50

2.6.1 Chemical Method 51

2.6.2 Temperature-swing Adsorption-desorption 54

2.7 Current Approaches for Removal of Chromium (III) Ions 57

2.7.1 Chemical Precipitation 57

2.7.2 Electrodialysis 58

2.7.3 Membrane Filtration 59

2.7.3 (a) Ultrafiltration (UF) 60

2.7.3 (b) Nanofiltration (NF) 60

2.8 Research Gap 62

**CHAPTER THREE: MATERIALS AND METHODS**


| | | | |
|---|---|---|---|
| 3.1 | Chemicals | | 65 |
| 3.2 | Flowchart of the Overall Experimental Works | | 67 |
| 3.3 | Preparation of PNIPAM-base / MNPs Composite Hydrogels | | 68 |
| | 3.3.1 | Preparation of MNPs via Co-precipitation Method | 68 |
| | 3.3.2 | Direct Polymerization of PNIPAM onto Bare MNPs | 69 |
| | 3.3.3 | Surface Modification of Bare MNPs via Silanization | 70 |
| | 3.3.4 | Polymerization of PNIPAM onto MPS-modified MNPs | 70 |
| | 3.3.5 | Silica Coating of bare MNPs | 70 |
| | 3.3.6 | Functionalization of MNPs with PVP | 71 |
| | 3.3.7 | Silica Coating of PVP-functionalized MNPs | 71 |
| | 3.3.8 | Synthesis of PNIPAM-silica-PVP-MNPs Composite Hydrogels | 71 |
| | 3.3.9 | Preparation of MPS-modified silica-PVP-MNPs | 72 |
| | 3.3.10 | Preparation of PNIPAM-MPS-silica-PVP-MNPs Composite Hydrogels | 72 |
| | 3.3.11 | Synthesis of Co-polymeric (PNIPAM-co-AA)-silica-PVP-MNPs Composite Hydrogels | 73 |
| 3.4 | Physio-chemical Properties Analyses of the Composite Hydrogels | | 73 |
| | 3.4.1 | Identification of Functional Groups and Chemical Properties Analysis | 73 |
| | 3.4.2 | Estimation of PNIPAM Loading of the Composite Hydrogels. | 74 |
| | 3.4.3 | Dynamic Light Scattering (DLS) | 74 |
| | 3.4.4 | Magnetophoresis Kinetics Measurement | 75 |
| | 3.4.5 | Transmission Electron Microscopy (TEM) | 75 |
| | 3.4.6 | X-ray Photoelectron Spectroscopy (XPS) | 75 |
| 3.5 | Chromium (III) Adsorption-desorption Study | | 76 |

3.5.1 Measurement of $Cr^{3+}$ concentration 76

3.5.2 Temperature-manipulated Adsorption-desorption Study 77

3.5.3 Adsorption mechanism study 77

3.5.3 (a) Langmuir Isotherm Model 78

3.5.3 (b) Freundlich Isotherm Model 79

3.5.3 (c) Dubinin-Radushkevich Isotherm Model 80

3.5.3 (d) Temkin Isotherm Model 81

3.5.3 (e) Flory-Huggins Isotherm Model 82

3.5.3 (f) Frumkin Isotherm Model 83

3.6 Adsorption Kinetics Study 85

**CHAPTER FOUR: RESULTS AND DISCUSSION**

4.1 Gelation of PNIPAM on bare MNPs 88

4.1.1 Structure of Co-precipitated Iron Oxide Magnetic Nanoparticles (MNPs) 89

4.1.2 Structure of PNIPAM-gelated MNPs Composites 90

4.1.3 Change in Thermo-responsive Behaviour of PNIPAM After Incorporation of MNPs 91

4.2 Surface Modification of MNPs via Silanization 94

4.2.1 Structure of PNIPAM-MPS-MNPs Composites 94

4.2.2 Thermo-responsive Behaviour of PNIPAM-gelated MPS-MNPs 96

4.2.3 Chemical Identification of the Composite Materials 99

4.2.4 Colloidal Stability Study 100

4.3 Stability Enhancement by Silica Coating of MNPs 103

4.3.1 Silica Coating on Bare MNPs 104

4.3.2 Pre-functionalization of MNPs by PVP for Effective Silica Coating 105

4.3.3 Surface Modification of Silica-coated PVP-MNPs by MPS 106

4.4 Gelation of PNIPAM on Silica-coated PVP-MNPs (with and without MPS) 107

4.5 Chemical Composition Change from Bare MNPs to PNIPAM-gelated MNPs Composite Hydrogels. 108

4.5.1 Thermal Stability of Layer-by-layer Coating 111

4.5.2 Thermo-responsive Volume Phase Transition 114

4.5.3 Surface Charge Variation Induced by Thermo-responsive Behaviour 116

4.5.4 Phase Separation Kinetics of Composite Hydrogels 117

4.5.5 Magnetophoresis Profiles of Composite Hydrogels 118

4.6 Physio-chemical Properties of Chromium-laden Hydrogels 124

4.6.1 Chemical Composition of Composite Hydrogels After $Cr^{3+}$ Adsorption 124

4.6.2 Post-adsorption Morphological Change 125

4.6.3 Surface Composition Change of Hydrogels After $Cr^{3+}$ Adsorption 126

4.6.4 Thermo-responsive Behaviour of Chromium-laden Composite Hydrogels. 128

4.6.5 Changes in Surface Potentials After Adsorption of $Cr^{3+}$ 130

4.6.6 Post-adsorption Colloidal Stability 131

4.7 $Cr^{3+}$ Adsorption Efficiency of PNIPAM-silica-PVP-MNPs Composite Hydrogels 133

4.7.1 Influence of Hydrogel Dosage on $Cr^{3+}$ Adsorption 134

4.7.2 Thermo-responsive Adsorption-desorption of $Cr^{3+}$ 134

4.7.3 Adsorption Mechanism of $Cr^{3+}$ 137

4.8 Enhancement of $Cr^{3+}$ Chelating Ability by Coupling with Acrylic Acid (AA). 141

4.8.1 Identification of Functional Groups as $Cr^{3+}$ Binding Moieties 142

4.8.2 Thermo-responsive Swelling-deswelling Behaviour Change in the Presence of AA 145

4.8.3 Surface Potential Change Before and After Adsorption of $Cr^{3+}$ 149

4.8.4 Kinetic of Phase Separation Before and After $Cr^{3+}$ Adsorption. 151

4.8.5 Magnetophoresis Kinetics Profiles Before and After $Cr^{3+}$ Adsorption. 152

4.8.6 Morphological Change Before and After $Cr^{3+}$ Adsorption 153

4.8.7 Surface Composition Change Before and After $Cr^{3+}$ Adsorption 155

4.9 $Cr^{3+}$ Adsorption Efficiency of (PNIPAM-co-AA)-silica-PVP-MNPs Composite Hydrogels 156

4.10 Thermo-responsive Adsorption-desorption of $Cr^{3+}$ by (PNIPAM-co-AA)-silica-PVP-MNPs Hydrogels 158

4.11 Adsorption Isotherm for (PNIPAM-co-AA)-silica-PVP-MNPs 160

4.12 Adsorption Kinetics of $Cr^{3+}$ 164

**CHAPTER FIVE: CONCLUSIONS AND RECOMMENDATIONS**

5.1 Conclusions 170

5.2 Recommendations 172

**REFERENCES** 174

**APPENDICES**

APPENDIX A Gelation of PNIPAM via Free-radical Polymerization

APPENDIX B UV-Spectrophotometer Calibration Curve for Chromium (III) Concentration Measurement.

APPENDIX C Sample Calculations for $Cr^{3+}$ Adsorption by Composite Hydrogels

**LIST OF PUBLICATIONS**

## LIST OF TABLES

**Page**


| | | |
|---|---|---|
| Table 2.1 | Lower critical solution temperature (LCST) of different thermos-responsive polymers | 23 |
| Table 2.2 | Comparisons in adsorption capacities of different biopolymer hydrogels for adsorption of different heavy metal ions | 44 |
| Table 2.3 | Comparisons in adsorption capacities of different synthetic polymer hydrogels for adsorption of different heavy metal ions | 49 |
| Table 3.1 | List of chemicals and reagents used | 66 |
| Table 3.2 | List of adsorption isotherm models used | 84 |
| Table 4.1 | Assignments of main spectral bands based on their atomic concentration (AC) for PNIPAM-silica-PVP-MNPs composite hydrogels before and after adsorption of $Cr^{3+}$ | 127 |
| Table 4.2 | Isotherm parameters for adsorption of $Cr^{3+}$ by PNIPAM-silica-PVP-MNPs composite hydrogels at different temperatures | 139 |
| Table 4.3 | Assignments of main spectral bands based on their atomic concentration (AC) for (PNIPAM-co-AA)-silica-PVP-MNPs composite hydrogels before and after adsorption of $Cr^{3+}$ | 156 |
| Table 4.4 | Isotherm parameters for adsorption of $Cr^{3+}$ by (PNIPAM-co-AA)-silica-PVP-MNPs composite hydrogels at different temperatures | 161 |
| Table 4.5 | Comparison of the pseudo-first-order, pseudo-second-order and intra-particle diffusion adsorption rate constants and the calculated and experimental $q_e$ values for PNIPAM-silica-PVP-MNPs and (PNIPAM-co-AA)-silica-PVP-MNPs composite hydrogels. ($T$ = 298 K, pH 5) | 167 |

## LIST OF FIGURES


| | | Page |
|---|---|---|
| Figure 2.1 | Figure 2.1: Schematic illustration of the swelling-shrinking behaviour of stimuli-responsive hydrogels | 21 |
| Figure 2.2 | Schematic illustration of the thermos-responsive phase transition of acrylamide-base polymer | 23 |
| Figure 2.3 | A) Chemical structure of poly(*N*-isopropylacrylamide) (PNIPAM); B) schematic illustration of the volume phase transition of cross-linked PNIPAM hydrogel | 24 |
| Figure 2.4 | Alignment of the magnetic moments of individual atoms in a MNP | 26 |
| Figure 2.5 | Schematic diagram of the preparation route of PNIPAM-encapsulated MNPs with MPS as surface modifying silane | 29 |
| Figure 2.6 | (a) PNIPAM-MNPs composite microgel formation mechanism for MNPs cluster larger than the nanogels, and (b) for MNPs cluster smaller than the nanogels | 31 |
| Figure 2.7 | Three different structural designs with uniform distribution of MNPs within hydrogel matrix: a) Stabilization of inorganic MNPs by a stabilizing hydrogel matrix, b) non-covalent immobilization of MNPs, and c) covalent immobilization of MNPs in a hydrogel matrix | 32 |
| Figure 2.8 | Schematic illustration of preparation route of MNPs-anchored PNIPAM-co-AA microcontainers | 34 |
| Figure 2.9 | Schematic illustration of; (a) The structure of homo-polymeric CS-GLA hydrogels and; (b) the proposed mechanism of pH-manipulated adsorption-desorption of $Cu^{2+}$ by GLA-cross-linked CS-PAA hybrid hydrogels | 42 |

| | | |
|---|---|---|
| Figure 2.10 | Illustration of the interactions between $Hg^{2+}$ ions and cross-linked AAm-CA hydrogels | 47 |
| Figure 2.11 | Schematic diagram illustrates the pH-manipulated recyclable application of thermo-responsive PNIPAM-P(NaAA) IPN hydrogels | 52 |
| Figure 2.12 | Schematic diagram of temperature-swing extraction of a metal ion complexed with an extractant onto the cross-linked PNIPAM hydrogels | 55 |
| Figure 2.13 | Schematic diagram illustrating the thermo-responsive adsorption-desorption behavior of P(NIPAM-co-BCAm) hydrogel towards $Pb^{2+}$ ions. The adsorption took place at temperature below the LCST, whereas the desorption occurred at temperature above the LCST | 56 |
| Figure 3.1 | Flowchart of the research works | 67 |
| Figure 4.1 | TEM images bare MNPs. Scale bars: 100 nm | 89 |
| Figure 4.2 | TEM images show that there are some darker patches which could possibly be the denser clusters of MNPs enveloped by PNIPAM matrix, whereas the rest of the MNPs are adhered around the darker patches: (a) scale bar: 500 nm; (b) scale bar: 200 nm. | 90 |
| Figure 4.3 | (a) Hydrodynamic diameter, $D_h$ change and; (b) Zeta potential, $\zeta$ change against temperature change for PNIPAM-MNPs composite hydrogels | 92 |
| Figure 4.4 | TEM images for: (a-b) MPS-modified MNPs (c-d) PNIPAM-MPS-MNPs. Scale bars: 500 nm for (a) and (c); 200 nm for (b) and (d) | 95 |
| Figure 4.5 | (a) Hydrodynamic diameter, $D_h$ change and; (b) Zeta potential, $\zeta$ change against temperature for PNIPAM-MPS-MNPs composite hydrogels | 97 |
| Figure 4.6 | FT-IR spectra shows layer-by-layer significant peak change from bare MNPs until PNIPAM-MPS-MNPs | 100 |

| | | |
|---|---|---|
| Figure 4.7 | (a) kinetic profiles without magnetic field and (b) magnetic separation kinetic profiles for bare MNPs, MPS-MNPs, PNIPAM-MNPs and PNIPAM-MPS-MNPs | 101 |
| Figure 4.8 | TEM image for coating of silica onto bare MNPs. Large aggregates were formed. Scale bar: 500 nm | 105 |
| Figure 4.9 | TEM images for silica-coated PVP-MNPs. Scale bars: 200 nm. | 105 |
| Figure 4.10 | TEM image for MPS-modified silica-PVP-MNPs. Scale bars: 200 nm | 106 |
| Figure 4.11 | TEM images for: (a-b) PNIPAM-silica-PVP-MNPs (c-d) PNIPAM-MPS-silica-MNPs. Scale bars: 500 nm for (a) and (c); 200 nm for (b) and (d) | 108 |
| Figure 4.12 | FT-IR spectra shows layer-by-layer significant peak change from bare MNPs until PNIPAM-MPS-silica-PVP-MNPs | 109 |
| Figure 4.13 | Schematic diagram shows the major steps involved in layer-by-layer coatings of both PNIPAM-silica-PVP-MNPs and PNIPAM-MPS-silica-PVP-MNPs composite hydrogels | 111 |
| Figure 4.14 | Layer-by-layer TGA curve change: (a) from bare MNPs to PNIPAM-silica-PVP-MNPs and; (b) from silica-PVP-MNPs to PNIPAM-MPS-silica-PVP-MNPs | 112 |
| Figure 4.15 | Hydrodynamic diameters, $D_h$ of; (a) PNIPAM-silica-PVP-MNPs and (b) PNIPAM-MPS-silica-PVP-MNPs nanoparticles as a function of temperature | 115 |
| Figure 4.16 | Zeta potential, $\zeta$ change over temperature variation for; (a) PNIPAM-silica-PVP-MNPs and (b) PNIPAM-MPS-silica-PVP-MNPs. | 117 |
| Figure 4.17 | Kinetic profiles without magnetic field for the samples beginning from bare MNPs until PNIPAM-MPS-silica-PVP-MNPs | 118 |

| | | |
|---|---|---|
| Figure 4.18 | Magnetic separation kinetic profiles for the samples beginning from bare MNPs until PNIPAM-MPS-silica-PVP-MNPs | 119 |
| Figure 4.19 | Comparison the collection rate of (left) bare MNPs and (right) silica–PVP–MNPs composites by a NdFeB magnet within 420 min. Both suspensions were prepared with concentration of 0.2 g $L^{-1}$. The brownish colour of bare MNPs suspension and muddy hue of silica-PVP-MNPs suspension had faded at nearly equal rate at the end of magnetic collection | 121 |
| Figure 4.20 | Comparison the collection rate of (left) PNIPAM-silica-PVP-MNPs and (right) silica–PVP–MNPs composites by a NdFeB magnet within 420 min. Both suspensions were prepared with concentration at 0.2 g $L^{-1}$. The suspension colour of silica-PVP-MNPs was observed to have faded more rapidly than its PNIPAM-gelated counterpart indicating PNIPAM polymeric networks enhanced the colloidal stability via interfacial steric repulsion | 122 |
| Figure 4.21 | Comparison the collection rate of (left) PNIPAM-silica-PVP-MNPs and (right) PNIPAM-MPS-silica–PVP–MNPs composite hydrogels by a NdFeB magnet within 420 min. Both suspensions were prepared with concentration at 2 g $L^{-1}$. The solute phase of PNIPAM-MPS-silica-PVP-MNPs was witnessed to be separated at higher rate. Larger particle size and higher polydispersity had collectively contributed to its higher vulnerability of being harvested by external magetic force | 123 |
| Figure 4.22 | FTIR spectrum shows comparisons in peak change before and after adsorption $Cr^{3+}$ for PNIPAM-silica-PVP-MNPs composite hydrogels | 125 |
| Figure 4.23 | TEM images of PNIPAM-silica-PVP-MNPs hydrogels: (a-b) before and (c-d) after $Cr^{3+}$ adsorption. Scale bars: 500 nm for (a) and (c) 200 nm for (b) and (d) | 126 |

| | | |
|---|---|---|
| Figure 4.24 | X-ray photoelectron spectroscopy (XPS) survey spectra of PNIPAM-silica-PVP-MNPs hydrogels before and after $Cr^{3+}$ adsorption | 127 |
| Figure 4.25 | Hydrodynamic diameter, $D_h$ change over temperature for PNIPAM-silica-PVP-MNPs after $Cr^{3+}$ adsorption ($C_0$ = 100 mg $L^{-1}$). | 129 |
| Figure 4.26 | Zeta potential, $\zeta$ change over temperature for PNIPAM-silica-PVP-MNPs after $Cr^{3+}$ adsorption ($C_0$ = 100 mg $L^{-1}$). | 131 |
| Figure 4.27 | Kinetic profiles without magnetic field and magnetic separation kinetic profiles for PNIPAM-silica-PVP-MNPs after $Cr^{3+}$ adsorption | 132 |
| Figure 4.28 | Effect of initial concentration of $Cr^{3+}$ on the adsorption of $Cr^{3+}$ onto PNIPAM-silica-PVP-MNPs composite hydrogels. ($pH$ = 5, $V$= 50 mL, $M$ = 4 mg, $T$ = 298 K) | 133 |
| Figure 4.29 | $Cr^{3+}$ adsorption with different PNIPAM-silica-PVP-MNPs composite hydrogel concentrations ($C_0$ = 100 mg $L^{-1}$, $V$ = 50 mL, $T$ = 298 K, pH = 5) | 134 |
| Figure 4.30 | Profile of $Cr^{3+}$ adsorption capacity, $q_e$ of PNIPAM-silica-PVP-MNPs composite hydrogels normalized by corresponding equilibrium concentration, $C_e$ at different temperatures against varying initial concentration, $C_0$. (Solution pH = 5) | 136 |
| Figure 4.31 | Comparison of experimental $Cr^{3+}$ adsorption capacity, $q_e$ with different plots of $q_e$ values calculated by various isotherm models against different equilibrium $Cr^{3+}$ concentrations, $C_e$. (pH = 5, $V$ = 50 mL, $M$ = 4 mg) | 138 |
| Figure 4.32 | Schematic diagram shows the thermos-responsive mechanisms for $Cr^{3+}$ ions adsorption by PNIPAM-silica-PVP-MNPs composite hydrogels. Chelation of diffused $Cr^{3+}$ dictated within hydrogel network | 141 |
| Figure 4.33 | FTIR spectrum shows comparisons in peak change before and after adsorption $Cr^{3+}$ for (PNIPAM-co-AA)-silica-PVP-MNPs magnetic core composite hydrogels | 143 |

| | | |
|---|---|---|
| Figure 4.34 | Layer-by-layer TGA curves change: (a) from bare MNPs to PNIPAM-silica-PVP-MNPs and; (b) from silica-PVP-MNPs to (PNIPAM-co-AA)-silica-PVP-MNPs | 144 |
| Figure 4.35 | Hydrodynamic diameter, $D_h$ change over temperature, $T$ for (PNIPAM-co-AA)-silica-PVP-MNPs; (a) before and (b) after $Cr^{3+}$ adsorption ($C_0$ = 100 mg $L^{-1}$). | 146 |
| Figure 4.36 | Zeta potential, $\zeta$ change over temperature, $T$ for (PNIPAM-co-AA)-silica-PVP-MNPs; (a) before and (b) after $Cr^{3+}$ adsorption ($C_0$ = 100 mg $L^{-1}$). | 150 |
| Figure 4.37 | Kinetic profiles without magnetic field for (PNIPAM-co-AA)-silica-PVP-MNPs before and after $Cr^{3+}$ adsorption | 152 |
| Figure 4.38 | Magnetic separation kinetic profiles for (PNIPAM-co-AA)-silica-PVP-MNPs before and after $Cr^{3+}$ adsorption | 153 |
| Figure 4.39 | TEM images for: (a-b) (PNIPAM-co-AA)-silica-PVP-MNPs before $Cr^{3+}$ adsorption (c-d) (PNIPAM-co-AA)-silica-PVP-MNPs after $Cr^{3+}$ adsorption. Scale bars: 500 nm for (a) and (c); 200 nm for (b) and (d) | 154 |
| Figure 4.40 | X-ray photoelectron spectroscopy (XPS) survey spectra of (PNIPAM-co-AA)-silica-PVP-MNPs hydrogels before and after $Cr^{3+}$ adsorption | 156 |
| Figure 4.41 | Effect of initial concentration of $Cr^{3+}$ on the adsorption of $Cr^{3+}$ onto (PNIPAM-co-AA)-silica-PVP-MNPs magnetic composite hydrogels. ($pH$ = 5, $V$ = 50 mL, $M$ = 4 mg, $T$ = 298 K) | 157 |
| Figure 4.42 | Profile of $Cr^{3+}$ adsorption capacity, $q_e$ of (PNIPAM-co-AA)-silica-PVP-MNPs normalized by corresponding equilibrium concentration, $C_e$ at different temperatures against varying initial concentration, $C_0$. (Solution pH = 5) | 158 |

| | | |
|---|---|---|
| Figure 4.43 | Comparison of experimental $Cr^{3+}$ adsorption capacity, $q_e$ with different plots of $q_e$ values calculated by various isotherm models against different equilibrium $Cr^{3+}$ concentrations, $C_e$. (pH = 5, $V$ = 50 mL, $M$ = 4 mg) | 162 |
| Figure 4.44 | Schematic diagram shows the thermos-responsive mechanisms for $Cr^{3+}$ ions adsorption by (PNIPAM-co-AA)-silica-PVP-MNPs hydrogels. Surface adsorption of $Cr^{3+}$ predominated as more inner hydrogen bonds were formed within hydrogel network | 164 |
| Figure 4.45 | Kinetic plots of both types of composite hydrogels for the models of; (a) pseudo-first-order, (b) pseudo-second-order and (c) intra-particle diffusion | 166 |

## LIST OF ABBREVIATIONS

| | |
|---|---|
| AA | Acrylic acid |
| AAm-CA | Acrylamide-crotonic acid |
| AAS | Acrylic acid shell |
| AC | Activated carbon |
| AEM | Aminoethyl methacrylate hydrochloride |
| $Ag^{+}$ | Silver (I) cation |
| APS | Ammonium persulfate |
| APTES | 3-Aminopropyltriethoxysilane |
| AS-MNPs | Amino modified silica-iron oxide magnetic nanoparticles |
| Au | Gold |
| 3-bt | 3-butenoic acid |
| $Ca(OH)_2$ | Lime (calcium hydroxide) |
| CCGO | Magnetic cyclodextrin-chitosan / graphene oxide |
| $Cd^{2+}$ | Cadmium (II) cation |
| CEC | Cation exchange capacity |
| $C_2H_4CONH$ | Acrylamide |
| $C_3H_8NH$ | Pyrrolidine |
| $C_4H_{10}NH$ | Piperidine |
| CM | Carboxymethylated |
| CM-β-CD-MNPs | Carboxymethyl-β-cyclodextrin (CM-β-CD) modified $Fe_3O_4$ nanoparticles |
| $Co^{2+}$ | Cobalt (II) cation |
| CO | Carbonyl group |
| CONH | Amide group |
| $COO^{-}$ | Carboxylate group |
| COOH | Carboxylic group |
| Cr | Chromium |
| $Cr^{3+}$ | Chromium (III) cation |
| $Cr^{6+}$ | Chromium (VI) cation |
| $CrC1_3 \cdot 6H_2O$ | Chromium (III) chloride hexahydrate |

| | |
|---|---|
| $CrN_3O_9 \cdot 9H_2O$ | Chromium (III) nitrate nonahydrate |
| $Cr(H_2O)_6^{3+}$ | Hexaaquachromium (III) cation |
| $Cr(OH)^{4-}$ | Tetrahydroxochromate (III) anion |
| $Cr(OH)_3$ | Chromium (III) hydroxide |
| $Cr_2(OH)_2^{4+}$ | Binuclear dihydroxochromium (III) cation |
| $Cr_3(OH)_4^{5+}$ | Trinuclear tetrahydroxochromium (III) cation |
| CS | Chitosan |
| CS | Core-shell |
| $Cs^+$ | Cesium (I) cation |
| CS-PAA | Chitosan-poly(acrylic acid) |
| CTAB | Cetyltrimethylammonium bromide |
| $Cu^{2+}$ | Copper (II) cation |
| DBS | n-dodecylbenzenesulfonic |
| $D_h$ | Hydrodynamic diameter |
| DLS | Dynamic light scattering |
| DNA | Deoxyribonucleic acid |
| ED | Electrodialysis |
| EDC·HCl | (3-dimethylaminopropyl) carbodiimide hydrochloride |
| EtOH | Ethanol |
| $Eu^{3+}$ | Europium (III) cation |
| FAU | Faujasites |
| $Fe^{2+}$ | Ferrous ion |
| $Fe^{3+}$ | Ferric ion |
| $Fe(acac)_3$ | Ferric acetylacetonate |
| $Fe_2(CrO_4)_3$ | Ferrous chromate |
| $Fe_3O_4$ | Magnetite |
| $\gamma$-$Fe_2O_3$ | Maghemite |
| FRP | Free radical polymerization |
| FT-IR | Fourier transform infrared spectroscopy |
| GLA | Glutaraldehyde |
| HAC | High adsorption capacities |
| HEMA | 2-Hydroxyethyl methacrylate |

| | |
|---|---|
| HCl | Hydrochloric acid |
| HEC-g-PAA | Hydroxylethyl cellulose-g-poly(acrylic acid) |
| $Hg^{2+}$ | Mercury (II) cation |
| $H_2O$ | Water |
| IDA | Iminodiacetic acid |
| IEP | Isoelectric point |
| IPN | Inter-penetrating networks |
| KPS | Potassium persulfate |
| LCST | Lower critical solution temperature |
| LOD | Limit of detection |
| MBA | *N*, *N*'-methylene-bis-acrylamide |
| MgO | Magnesium Oxide |
| MC | Merocyanine |
| MNPs | Iron Oxide Magnetic Nanoparticles |
| MPS | 3-(trimethoxysilyl)propyl methacrylate |
| MW | Molecular weight |
| MWCO | Molecular weight cut-off |
| $NaNO_3$ | Sodium nitrate |
| NaOH | Sodium hydroxide |
| $Na_2SO_4$ | Sodium sulfate |
| NF | Nanofiltration |
| $Ni^{2+}$ | Nickel (II) cation |
| NIPAM | *N*-isopropylacrylamide |
| NH | Amine group |
| NHS | N-hydroxysuccinimide |
| OH | Hydroxyl group |
| PAA | Poly(acrylic acid) |
| PAAm-HAp | Polyacrylamide-hydroxyapatite |
| PAC / PEG | Polyacrylate / poly(ethylene glycol) |
| P(AMPS-co-GT)-GO | Poly[(2-acrylamido-2-methyl propanesulfonic acid)-co-gum tragacanth] grafted graphene oxide composite |

| | |
|---|---|
| P(AMPS-co-IA) | Poly[2-(acrylamido)-2-methyl-1-propanesulfonic acid-co-itaconic acid] |
| $Pb^{2+}$ | Lead (II) cation |
| PEDOT / PSS | Lignin-poly(3,4-ethylenedioxythiophene) / polystyrene sulfonate |
| PEGDA | Poly(ethyelene glycol) diacrylate |
| PNaAA | Poly(sodium acrylate) |
| PNIPAM | Poly(*N*-isopropylacrylamide) |
| PNIPAM-co-AA | Poly(*N*-isopropylacrylamide-co-acrylic acid) |
| (PNIPAM-co-AA)-silica-PVP-MNPs | Poly(*N*-isopropylacrylamide-co-acrylic acid)-gelated silica- poly(vinylpyrrolidone)-iron oxide magnetic nanoparticles composite hydrogel |
| PNIPAM-co-AAm-co-MA | Poly(*N*-isopropylacrylamide-co-acrylamide-co-maleic acid) |
| P(NIPAM-co-BCAm) | Poly(*N*-isopropylacrylamide-co-benzo-18-crown-6-acrylamide) |
| PNIPAM-silica-PVP-MNPs | Poly(*N*-isopropylacrylamide)-gelated silica-poly(vinylpyrrolidone)-iron oxide magnetic nanoparticles composite hydrogel |
| PSt | Polystyrene |
| P(St-NIPAM) | Poly(styrene-*N*-isopropylacrylamide) |
| PSt-PNIPAM | Polystyrene-poly(*N*-isopropylacrylamide) |
| PVP | Poly(vinylpyrrolidone) |
| P(4-VP-co-HEMA) | Poly(4-vinyl pyridine-co- 2-hydroxyethylmetacrylate) |
| $SCH_2COOH$ | Thiodiglycolic acid |
| SDBS | Sodium n-dodecylbenzenesulfonate |
| SH | Sodium humate |
| silica | Silica coating layer |
| SiOH | Silanol |
| SiOSi | Siloxane |
| $SO_3H$ | Sulfonic acid |
| SP | Spiropyran |

| | |
|---|---|
| SP-PNVCL | Spiropyran-ended poly(N-vinyl caprolactam) |
| $Sr^{2+}$ | Strontium (II) cation |
| St | Starch |
| TEOS | Tetraethyl orthosilicate |
| $Th^{4+}$ | Thorium (IV) cation |
| THF | Tetrahydrofuran |
| TS-SPE | Temperature-swing solid-phase extraction |
| $U^{6+}$ | Uranium (VI) cation |
| UF | Ultrafiltration |
| $UO_2^{2+}$ | Uranyl cation |
| UV | Ultraviolet |
| UV-Vis | Ultraviolet-visible |
| V50 | 2,2’-Azobis(2-amidinopropane) dihydrochloride |
| VIM | *n*-vinyl imidazole |
| VPT | Volume phase transition |
| VPTT | Volume phase transition temperature |
| $Zn^{2+}$ | Zinc (II) cation |

## LIST OF SYMBOLS

| | |
|---|---|
| $T$ | Temperature (°C and K) |
| $pK_a$ | Acid dissociation constant |
| $pK_b$ | Base dissociation constant |
| $D_h$ | Hydrodynamic diameter (nm) |
| $\zeta$ | Zeta potential (mV) |
| $R$ | $Cr^{3+}$ removal percentage (%) |
| $C_0$ | Initial concentration of copper (II) cations in solution (mg $L^{-1}$) |
| $C_e$ | Equilibrium concentration in solution (mg $L^{-1}$) |
| $M$ | Dry mass of adsorbent (g) |
| $V$ | Total volume of solution (L) |
| $q_e$ | Equilibrium adsorption capacity (mg $g^{-1}$) |
| $q_m$ | Maximum equilibrium adsorption capacity (mg $g^{-1}$) |
| $q_t$ | Equilirium adsorption capacity at time $t$ (mg $g^{-1}$) |
| $K_L$ | Langmuir constant (L $mg^{-1}$) |
| $R_L$ | Langmuir separation factor |
| $K_F$ | Freundlich constant (L $g^{-1}$) |
| $1/n$ | Freundlich heterogeneity factor |
| $B$ | Dubinin-Radushkevich constant related to adsorption energy ($mol^2$ $k^{-1}J^{-2}$) |
| $R$ | Gas constant (8.314 J $mol^{\cdot -1}K^{-1}$) |
| $\varepsilon$ | Polanyi potential |

| | |
|---|---|
| $E$ | Free mean energy of the adsorption (kJ $mol^{-1}$) |
| $b$ | Temkin constant related to heat of adsorption (J $mol^{-1}$) |
| $K_T$ | Temkin constant (L $g^{-1}$) |
| $\theta$ | Degree of surface coverage by adsorbates |
| $K_{FH}$ | Flory-Huggins equilibrium constant (L $g^{-1}$) |
| $n$ | Flory-Huggins model exponent |
| $\Delta G^o$ | Standard free energy change (kJ $mol^{-1}$) |
| $K_{FR}$ | Frumkin equilibrium constant (L $g^{-1}$) |
| $a$ | interaction parameter related to the interaction energy of the adsorbates |
| $k_1$ | Pseudo-first-order rate constant ($min^{-1}$) |
| $k_2$ | Pseudo-second-order rate constant (g $mg^{-1}$ $min^{-1}$) |
| $k_{id}$ | Intra-particle diffusion rate constant (mg $g^{-1}min^{-1/2}$) |
| $C_{id}$ | Constant related to the thickness of the boundary layer (mg $g^{-1}$) |

**SINTESIS HIDROGEL KOMPOSIT BERASASKAN POLI(*N*-ISOPROPILAKRILAMID) YANG BERSIFAT TERMO-MAGNETO-RESPONSIF UNTUK PENJERAPAN-NYAH PENJERAPAN ION-ION KROMIUM (III)**

## ABSTRAK

Hidrogel komposit yang bersifat perangsang-responsif telahpun menjadi perintis penyelidikan untuk aplikasi mereka dalam penjerapan dan pelepasan ion logam melalui perubahan bentuk. Penyediaan hidrogel komposit yang bersifat termo- dan magnet-responsif memerlukan penglitupan teras nanozarah magnet ferum oksida (MNPs) dengan petala berfungsi secara lapisan-demi-lapisan. Namun begitu, penyalutan berpetala MNPs yang berbilang peringkat menjadi penghalang utama dalam penghasilan hidrogel-hidrogel komposit yang mempunyai kestabilan koloid mantap dan sifat dwi-responsif yang berfungsi dengan baik. Dalam kajian ini, hidrogel-hidrogel komposit bertautsilang MNPs bersalutkan homo-polimer poli (*N*-isopropilakrilamid) (PNIPAM-MNPs) telah disintesiskan secara mudahnya melalui penglitupan lapisan-demi-lapisan dengan tanpa menggunakan pelopor silana, 3-(trimetoksisilil)propil metakrilat (MPS). Ini didapati bahawa PNIPAM boleh digelkan terus ke atas MNPs berfungsian polivinilpirolidon (PVP) yang telah dilitupi silika (silika-PVP-MNPs) melalui pempolimeran radikal bebas tanpa penggunaan MPS untuk menambahbaikkan kestabilan koloid dan sifat termo-magneto-responsif. Selain itu, hidrogel komposit MNPs bersalutkan ko-polimer poli(*N*-isopropilacrilamid-ko-asid akrilik) [(PNIPAM-ko-AA)-silika-PVP-MNPs] dihasilkan demi menunjukkan perbezaan dalam mekanisme penjerapan antara kumpulan-kumpulan pengkelat karboksilat (-$COO^-$) terkandung dalam moieti AA dan amid-amid (-CONH) dalam moieti NIPAM. Dalam ujian penjerapan-nyahpenjerapan di bawah manipulasi suhu,

nyahpenjerapan $Cr^{3+}$ menjadi semakin ketara selaras dengan peningkatan suhu daripada 298 K sehingga 323 K bagi PNIPAM-silica-PVP-MNPs. Penjerapan semula $Cr^{3+}$ berlaku semasa hidrogel-hidrogel komposit tersebut dilindap ke suhu 298 K untuk kepekatan permulaan $Cr^{3+}$ yang lebih rendah (20 – 80 mg $L^{-1}$) telah menunjukkan bahawa nyahpenjerapan dapat dikecapi untuk penjerapan permukaan. Sebelum pemanasan, data penjerapan keseimbangan $Cr^{3+}$ dapat dipadankan dengan baik dalam model Flory-Huggins dan Frumkin, menunjukkan bahawa pengkelatan ion-ion $Cr^{3+}$ berlaku melalui penggantian molekul-molekul air pada tapak pengikat. Tambahan pula, PNIPAM-silika-PVP-MNPs mempunyai kapasiti penjerapan maksimum, $q_m$ (434.78 mg $g^{-1}$) yang lebih tinggi berbanding dengan (PNIPAM-ko-AA)-silika-PVP-MNPs ($q_m$ = 243.90 mg $g^{-1}$) seperti yang diekstrapolasikan daripada model isoterma Langmuir bahawa kedua-dua hydrogel komposit telah menunjukkan pemadanan yang baik dalam model tersebut. Analisis kinetik penjerapan pula menunjukkan bahawa penjerapan $Cr^{3+}$ pada PNIPAM-silika-PVP-MNPs tertakluk pada resapan intra-zarah serta penjerapan fizikal berbalik kerana data-data hydrogel itu mengikuti model pseudo-pertama, pseudo-kedua dan resapan intra-zarah. Di samping itu, penjerapan kimia permukaan adalah dominan untuk (PNIPAM-ko-AA)-silika-PVP-MNPs kerana hydrogel ini hanya mengikuti model pseudo-kedua.

**SYNTHESIS OF THERMO-MAGNETO-RESPONSIVE POLY(*N*-ISOPROPYLACRYLAMIDE)-BASED COMPOSITE HYDROGELS FOR ADSORPTION-DESORPTION OF CHROMIUM (III) IONS.**

## ABSTRACT

Stimuli-responsive composite hydrogels have been in the vanguard of researches for their application in metal ion adsorption and its release via conformational change. The preparation of composite hydrogels with both thermo- and magneto-responsiveness requires careful layer-by-layer coatings of functional shells onto the core of iron oxide magnetic nanoparticles (MNPs). However, multiple stages of shell encapsulation of MNPs remains a major setback on the production of composite hydrogels with adequate colloidal stability and well-functioned dual-responsiveness. In this study, homo-polymeric poly(*N*-isopropylacrylamide)-encapsulated magnetite nanoparticles (PNIPAM-MNPs) cross-linked composite hydrogels were facilely synthesized via layer-by-layer coatings with and without employing silanization precursor, 3-(trimethoxysilyl)propyl methacrylate (MPS). It was found that PNIPAM could be gelated directly onto the silica-coated, poly(vinylpyrrolidone) (PVP) functionalized MNPs (silica-PVP-MNPs) via free radical polymerization without MPS to improve its colloidal stability and both thermo-magneto-responsive. Besides, co-polymeric poly(*N*-isopropylacrylamide-co-acrylic acid)-encapsulated MNPs ((PNIPAM-co-AA)-silica-PVP-MNPs) composite hydrogels were prepared for elucidating the difference in adsorption mechanisms between chelating groups of carboyxlates ($-COO^-$) contained by AA moiety and amides (-CONH) of NIPAM moiety. In the temperature manipulated adsorption-desorption tests, desorption of $Cr^{3+}$ gradually predominated as temperature increased from 298 K to 323 K for PNIPAM-

silica-PVP-MNPs. Re-adsorption of $Cr^{3+}$ by the composite hydrogel took place as being quenched to 298 K for lower initial $Cr^{3+}$ concentration (20 – 80 mg $L^{-1}$) which showed that desorption can be realised for surface adsorption. Before heating, the equilibrium adsorption data of $Cr^{3+}$ fitted well into Flory-Huggins and Frumkin models, that elucidated the chelation of $Cr^{3+}$ ions occurred via replacement of water molecules on the binding sites. Moreover, PNIPAM-silica-PVP-MNPs had higher maximum adsorption capacity, $q_m$ (434.78 mg $g^{-1}$) compared to (PNIPAM-co-AA)-silica-PVP-MNPs ($q_m$ = 243.90 mg $g^{-1}$) as extrapolated by Langmuir isotherm model in which the data of both composite hydrogels also showed good fit to the model. The adsorption kinetic analysis indicated that $Cr^{3+}$ adsorption on PNIPAM-silica-PVP-MNPs was governed by intra-particle diffusion and reversible surface physisorption as its data followed pseudo-first, pseudo-second- and intra-particle diffusion models. On the other hand, surface chemisorption predominated over (PNIPAM-co-AA)-silica-PVP-MNPs as it followed only pseudo-second model.

# CHAPTER ONE

# INTRODUCTION

## 1.1 Research Overview

Poly(*N*-isopropylacylamide) (PNIPAM) is known as a type of smart hydrogel that is sensitive to temperature variation in which its responsiveness towards temperature is manifested by conformational change of its cross-linked matrices. In recent years, there have been some attempts of introducing magneto-responsiveness via encapsulation of inorganic magnetic iron oxide ($Fe_3O_4$) nanoparticles (MNPs) into PNIPAM matrices to generate dual-responsive core-shell PNIPAM-MNPs composite hydrogels.

The collective behaviour of the dual-responsiveness rendered by this type of hybrid composite hydrogels provides several benefits for metal ion chelation, removal as well as recovery. The PNIPAM matrix shell acts as chelating agent for the metal ions whereas the thermo-responsiveness grants the PNIPAM shell with the ability to manipulate absorption and release of the metal ions from the polymer matrices under temperature variation. Moreover, the magneto-responsive core permits facile separation of hydrogels from its bulk phase by a magnet without resorting to centrifugation and chemical precipitation that are energy inefficient and not environmentally friendly, respectively.

Regeneration of the composite hydrogels as reusable adsorbents can also be achieved by tunable hydrophilicity of the hydrogels as a function of temperature. The transition between uptake and release of targeted ions corresponds to the temperature-manipulated change in hydrogel hydrophilicity as temperature varies within a narrow

range across the hydrogel lower critical solution temperature (LCST). The synergistic mechanisms of thermo-responsive adsorption-desorption of metal ions and magneto-responsive solute phase separation are expected to enhance the efficiency of the controlled uptake-release of metal ions (Morris *et al.*, 1997, Yamashita *et al.*, 2003).

## 1.2 Thermo-responsive Composite Hydrogels for Heavy Metal Removal

Stimuli-responsive polymeric hydrogel is defined as a three-dimensional network structure of cross-linked polymer chains that undergoes volume phase transition (VPT) in response to the triggering effect of external stimuli such as temperature, solution pH and electrical field. The VPT mechanism is characterized by the swelling-shrinking behaviour of the hydrogel networks which is in turn actuated by the tendency of the hydrogels to imbibe (swelling) and to expel (shrinking) water in aqueous solution. The water absorbing ability is contributed by the hydrophilic functionalities such as amide ($-CONH_2$), carboxyl (-COOH) and hydroxyl (-OH) contained within the hydrogel structures. Hence, this type of stimuli-responsive hydrogels is also coined “smart” or “intelligent” gels ascribed to their flexibility in conformational change (Pelton, 2000, Burmistrova et al., 2011, Sun et al., 2011).

Among a vast diversity of stimuli-responsive polymers, hydrogels formed by cross-linked thermo-responsive PNIPAM polymer backbones (chains) with interesting physio-chemical flexibility have emerged as one of the most popular types of its kind to be intensively studied. The earliest synthesis of thermo-responsive PNIPAM hydrogels was reported by Pelton and Chibante (1986). Since then, it has been drawing tremendous attention from researchers of various disciplines to delve into the feasibility of these hydrogels to be utilized in extensive applications including

biomedical engineering, drug delivery and wastewater treatments (Pelton and Chibante, 1986, Morris et al., 1997, Ju et al., 2009, Burmistrova et al., 2011)

Thermo-responsive PNIPAM hydrogels exhibit VPT when the temperature of its environment increases above its volume phase transition temperature (VPTT), which is equivalent to the lower critical solution temperature (LCST) of PNIPAM chains for the cases where the PNIPAM hydrogels are homo-polymeric in composition. Below the VPTT, water is absorbed into the hydrogel interiors to cause swelling because hydrophilic groups of the hydrogels are exposed and hydrated. As temperature rises above VPTT, dehydration takes place, water-associated hydrogen bonds are broken and water is released from the hydrogel matrices causing the network structure to shrink into collapsed state (Morris et al., 1997, Saunders and Vincent, 1999, Pelton, 2000, Zhang and Wang, 2009, Sun et al., 2011).

Interestingly, the hydrophilic functional moiety responsible for thermo-responsive VPT of PNIPAM hydrogels (amide) also possesses metal ion-recognition quality which endows the hydrogels with ion-chelating ability to adsorb targeted ions including multivalent heavy metal ions in aqueous solution. Hence, the thermo-responsive swelling-shrinking behaviour of PNIPAM hydrogels could be utilized as a novel mechanism for effective adsorption and desorption of metal ions. In principles, metal ions from the bulk phase is expected to have diffused into hydrogel interiors driven by concentration gradient and being chelated by the binding groups at temperature below VPTT. Upon increase in temperature beyond VPTT, the enthalpy-driven dehydration and structural shrinkage facilitates the release of water in unison with the metal ions from the shrunken hydrogel matrices.

The controlled uptake-release of metal ions by PNIPAM hydrogels via thermo-responsive swelling-shrinking mechanistic has the advantage of preventing pollution problem arose from chemical recovery of metal ions by pH adjustment. Besides, the regeneration of hydrogels as adsorbents can also be achieved by manipulation of temperature. Nonetheless, in the contexts of practical application as adsorbents, they still need further improvement on the low adsorption capacity and selectivity (Morris et al., 1997, Pan et al., 2009, Zhao et al., 2011).

The problem of low adsorption capacity of the hydrogels towards targeted ions can be solved by tailoring addition of co-monomers such as acrylic acids and sulfonic acids with strong chelating groups into the hydrogel skeletons. Nevertheless, the introduction of co-monomers is a double-edged sword, on one hand, it increases the density of the ion-recognition functionalities along the hydrogel skeletons. On the other hand, these hydrophilic groups prone to be hydrated by water molecules resulting in higher swelling-shrinking ratio which impoverishes the mechanical stability of the hydrogel structures. Again, the increased hydrophilicity also creates resistance against metal ions diffusion into the hydrogel matrices (Pan et al., 2009, Zhao et al., 2018).

In the recent years, avalanche of ideas has been attempted by researchers to improve adsorption performance of polymeric hydrogels, their mechanical stability and regeneration efficiency. Among multitude of techniques, the incorporation of magnetic nanoparticles (MNPs) such as superparamagnetic iron oxides into the cross-linked hydrogel hosts has been considered as an effective strategy to obtain polymer-based composite hydrogels. The incorporated MNPs is deemed to fortify the mechanical strength of the hydrogel hosts by acting as gelation seeds or being dispersed as non-covalently within the polymeric matrices. Moreover, the formed MNPs-hydrogel composites retain not only the favourable properties of pure hydrogels,

but also enhanced efficiency of solutes collection by magnetic phase separation. The collection of reaction solutes can be performed in an environmentally friendly way instead of using conventional approach of chemical precipitation. The latter invites critical problem of secondary sludge and the used adsorbents are hardly regenerative (Deng et al., 2003, Ho and Li, 2008, Lien and Wu, 2008, Zhang and Wang, 2009, Li et al., 2010).

### 1.3 Polydispersity and Undesired Aggregation of Composite Hydrogels

Homo-polymeric PNIPAM hydrogels having regular shape, colloidal stability and narrow size distribution can be produced by facile free-radical polymerization involving generation of free radicals by initiator to initiate the polymerization of monomers and the formed polymer chains are cross-linked into gel network structures. This entire polymer gel formation process is also known as gelation. Basically, the recipe of PNIPAM gelation comprises of three essential components, namely: soluble *N*-isopropylacrylamide (NIPAM) as monomer, cross-linking agent, *N*, *N*'-methylene-bis-acrylamide (MBA) and persulfates as initiators.

However, the introduction of inorganic MNPs into the organic hydrogel host matrices to produce composite particles with adequate colloidal stability in suspension, shape regularity as well as low polydispersity has instead remained technically challenging. This is mainly because the incorporation of MNPs into polymeric hydrogel matrices by either in-situ encapsulation or post-gelation embedding techniques could easily disrupt the regular structures of the hydrogel matrices that end up composite products of undesirably polydisperse and colloidally unstable aggregates (Yang et al., 2009, Zhang and Wang, 2009, Luo et al., 2010).

In the case of in-situ encapsulation of MNPs during PNIPAM gelation, the polymerization of NIPAM monomers and the sulfate ($SO_4^-$) anions from initiators increase the ionic strength in the reaction solution which lead to destabilization of MNPs in the aqueous phase. Also, the reaction solution pH is approaching the isoelectric point (ISP) of the MNPs which could deteriorate inter-particle repulsion causing unwanted aggregation of MNPs. The aggregation is further fostered by magnetic dipole-dipole interaction. As a result, the hydrogel network could have been deposited on heterogeneous clusters of MNPs forming polydisperse composite colloids with indistinct shapes and colloidally unstable.

On the other hand, the post-gelation deposition of MNPs onto hydrogel cross-linked networks has similarly thorny drawback where the MNPs are distributed within hydrogel skeletons via non-covalent embedding. The weak non-covalent interactions risk detachments of MNPs from the hydrogel hosts under the effect of swelling-shrinking mechanism. In addition, uneven distribution and density of deposited MNPs on hydrogel surfaces could also increase the tendency of inter-particle aggregation fueled by both magnetic dipole-dipole as well as Van der Waals interactions. After all, stabilization problem has persisted as the most critical setback for the fabrication of magnetic PNIPAM-base composite hydrogels with desired design and physio-chemical properties (Ho and Li, 2008, Du et al., 2009, Luo et al., 2010).

### 1.4 Release of Metal Ions and Regeneration of the Composite Hydrogels

In general, there are several challenges faced by most researchers for employing polymeric hydrogels as nano-adsorbents for heavy metal ions adsorption. First and foremost, the regeneration problem of the hydrogels has always been the primary drawback which diminishes the charm of hydrogel as promising candidate for

adsorption. Most of the polymeric hydrogels, especially pH-responsive type requires chemical method for the recovery of adsorbed ions from the interior structures back into the bulk phase.

Prior to adsorption, functional chelating groups like carboxylic, amides and hydroxyl need to be oxidized (deprotonated) into Lewis conjugate bases for effective binding of targeted metal ions which is usually achieved by pH adjustment. Likewise, the recovery of adsorbed metal ions and regeneration of hydrogels can only be achieved by tuning solution pH to control the degree of oxidation-reduction of the ion-recognizing groups by either $OH^-$ of alkaline or $H^+$ of acids used. After all, this chemical ways of desorbing metal ions may promote undesired agglomeration of solutes as pH is lowered close to the isoelectric point (IEP) of PNIPAM hydrogels. The pH-induced aggregation hinders regeneration of hydrogel adsorbents. With that, the process also produces unwanted precipitates that can contaminate the solution as well as create sludge problem (Wu and Tian, 2008, Ju et al., 2009, Mizoguchi et al., 2010, Cerar, 2015).

## 1.5 Chromium and Its Interaction with PNIPAM

Chromium (Cr) is an element which has atomic weight of 51.966 g $mol^{-1}$ with specific gravity of 7.14. It has widespread applications in many industrial activities including metallurgy especially steel and alloy manufacturing, chemical manufacturing (dyes, electroplating, tanning), pulp production and mining (ore refining). The form of existence, and concentration of Cr in discharged effluents depend mainly on the Cr compounds utilized in the industrial process, the pH, and the presence of other organic and inorganic processing wastes. Most ubiquitously, Cr exists in trivalent $Cr^{3+}$ and hexavalent $Cr^{6+}$ states. The former is an important

component in most biological bodies and waterbodies, but its hexavalent counterpart is relatively toxic to animals. Long-term accumulation of $Cr^{6+}$ substances may lead to chronic diseases like lung cancer, kidney failure, irritation and inflammation to respiratory tract and eyes. Hence, it is vital to have insights of chromium speciation before an appropriate remedial strategy can be devised to remove it efficiently from wastewaters (Weckhuysen et al., 1996, Sharma et al., 2008, Mitra et al., 2017).

In general, trivalent $Cr^{3+}$ exists as hexa-aqua chromium (III) complex ion, $Cr(H_2O)_6^{3+}$ which is a strong acid with p$K_a$ ~ 4. The hexa-aqua $Cr^{3+}$ ions tend to undergo hydrolysis as pH increases above its p$K_a$ from 4 to 10 that results in the formation of polynuclear hydroxo species containing hydroxide ($OH^-$) bridges. It happens when the coordinated water molecules were deprotonated and being replaced by coordination of $OH^-$. As a result, there is a medley of $Cr^{3+}$ hydroxo species encompassing mono-nuclear $Cr(OH)^{2+}$, $Cr(OH)^3$, $Cr(OH)^{4-}$; dinuclear $Cr_2(OH)_2^{4+}$ and trinuclear $Cr_3(OH)_4^{5+}$ where each of these hydroxo species predominates at different pH under basic range depending on their degree of hydrolysis (Weckhuysen et al., 1996).

These $Cr^{3+}$ hydroxo complex cations (conjugate acids) are bound by anionic chelating groups (conjugate bases) of PNIPAM hydrogels to form Cr-chelator complexes. For instance, the amino (-NH) and carbonyl (-C=O) groups of amide moiety bind with the chromium hydroxo cation, one of the water ($H_2O$) molecules coordinated with the $Cr^{3+}$ is substituted by the hydrogel ligands to form ligand-chromium complex (Carbonaro and Stone, 2005, Girma et al., 2005, Petrou et al., 2010, Resende et al., 2014).

## 1.6 Problem Statement

In this study, thermo-magneto-responsive PNIPAM composite hydrogels were synthesized via layer-by-layer coating of MNPs. The multi-stage fabrication of the composite hydrogels consists of different functional steps aims to constitute dual-responsive composite hydrogels with core-shell structures. Nonetheless, incorporation of MNPs as magnetic cores into PNIPAM cross-linked matrix has always been technically challenging in the context of maintaining a desired balance among physio-chemical properties of the produced composite hydrogels including their colloidal stability, particle size distribution and dual-responsive nature that are critically important for their functional applications in heavy metal ions adsorption.

Although the multi-stage pre-treatment of MNPs cores has an ultimate purpose of preparing bare MNPs into colloidally stable and reactive template seeds for gelation of PNIPAM matrix, it also adds complications to the entire process flow of developing the desired composite products. Bare MNPs have high surface-to-volume ratio and surface energies which also endows high tendency to aggregate into clusters under the effect of magnetic dipole attraction. Hence, in most cases, MNPs are pre-coated by rigid silica ($SiO_2$) layer to impose colloidal stabilization. Silica coating also helps promote the compatibility between organic PNIPAM matrix and the inorganic MNPs cores. Despites this, envelopment of MNPs by silica shell provides robust seed skeleton with mechanical stability for the formation of well-defined core-shell structure prior to gelation of the organic polymeric matrix (Khrenov et al., 2007, Li et al., 2010).

Nonetheless, direct coating of silica layer onto bare MNPs via conventional Stöber method invites MNPs agglomeration problem as MNPs have poor dispersibility

in the reaction solvent. The magnetic MNPs could not be dispersed homogeneously in basic ethanol-ammonia mixture solvent because the pH is much closer to the IEP of MNPs than in the initial bare MNPs fluid. The magnetic attractions could overcome the interfacial repulsion between MNPs (Philipse et al., 1994, Graf et al., 2003, Sun et al., 2005). Hence, in this study, freshly co-precipitated bare MNPs were pre-functionalized with poly(vinylpyrrolidone) (PVP) as MNPs stabilizing polymer in Stöber reaction solvent as much as bridging agent to entail effective silica coating. The carbonyl (-C=O) groups of surface PVP could mediate formation of bridging linkages between silanols (-SiOH) of silica and hydroxyls of MNPs (Cha et al., 2010, Arsalani et al., 2010, Liberman et al., 2014).

In most previous cases, silane has been widely used as coupling agent to enhance adhesion compatibility between organic polymer and inorganic nanoparticle surfaces. Among avalanche of silane types, a type of alkoxysilane, 3-(trimethoxysilyl)propyl methacrylate (MPS) has also been used specifically for surface modification of MNPs. MPS carries terminal vinyl (-C=C-) groups with double bonds which can react with NIPAM monomer to allow the growth of PNIPAM polymers on the seed surfaces. However, MPS has a drawback of increasing interfacial adhesiveness of the MNPs, especially in aqueous solution. This increases the inclination of MNPs to self-assemble into aggregates during polymerization of PNIPAM which adds to the complication on controlling the formation of desired structures of the end composite products. Hence, in this research work, the possibility of directly gelating the PNIPAM cross-linked network onto silica-coated MNPs without silanization was proposed and the silica-coated MNPs were impregnated into hydrogel matrix via hydrogen bonding.

In the context of metal ions adsorption and recovery, most of the nanoadsorbents require chemical method of desorption process from adsorbent structures. pH adjustment remains the most utilized way of tuning the uptake and release extent of targeted ions by the adsorbents. However, there are several critical issues arose from the method that include; the recovered metal ions may form insoluble precipitates requiring post-adsorption treatment of sludges. Second, the structural inflexibility of most conventional adsorbents has problem of irreversible blocking of ion-recognition functionalities by adsorbed ions that cannot be regenerated by pH control for further use.

Hence, in view of mitigating the aforementioned issues, the thermo-responsive PNIPAM matrix of the composite hydrogels plays the part. PNIPAM exhibits thermo-reversible VPT upon variation within a narrow range of temperatures across its LCST. The hydrophilic amine ($-NH_2$) and carbonyl (-C=O) groups of amide moiety present in PNIPAM skeleton contribute to the conformational change via formation and dissociation of water-linked hydrogen bonds. On the other hand, these functional groups also act as ligands for chelating metal ions within hydrogel matrix. In principle, their thermo-responsive conformational swelling-shrinking mechanism can be utilized for thermally actuated adsorption and desorption of metal ions without changing phase homogeneity of the targeted ions and the need of chemical addition. This hypothesis requires further investigation on its viability for thermal actuated uptake-release of metal ions in the research works (Morris et al., 1997, Yamashita et al., 2003, Ju et al., 2009, Mizoguchi et al., 2010).

In terms of separation, pure PNIPAM hydrogels are considerably stable in suspension and well-dissolved in aqueous phase at swollen state, mechanical separation of hydrogels from solution phase like centrifugation at room temperature is

not favourably feasible. Hence, paramagnetic MNPs enveloped inside PNIPAM matrix act as the magneto-responsive component which facilitates the post-adsorption phase separation of the composite hydrogels by an external magnetic field. As mentioned above, complications on incorporation of MNPs into hydrogel structures to produce core-shell composite structures that are colloidally stable with well-functioned dual-responsiveness remains the major issue in this study (Ho and Li, 2008, Du et al., 2009, Luo et al., 2010).

Apart from that, the metal adsorption capacity of homo-polymeric PNIPAM hydrogels is limited by the density and the affinity of functional groups available for metal ion chelation. Addition of co-monomer with reactive metal ion recognizing groups like acrylic acid (AA) into the hydrogel skeleton could enhance the adsorption capacity of the composite hydrogels. However, high content of AA also increases the tendency for the formation of more inner hydrogen bonds which may impair the reversibility of swelling-shrinking behaviour and the adsorption-desorption capacity could adversely impacted. Hence, the detailed investigation on this implication is necessary to be performed.

## 1.7 Research Objectives

The aim of this research work is to quest for the facile method of developing magnetic nanoparticles (MNPs) embedded PNIPAM composite hydrogels possessing thermo-magneto-responsive behaviour that can be utilized for effective temperature-swing adsorption-desorption of $Cr^{3+}$ ions in aqueous solutions. The objectives of this study are outlined as follows:

1) To study different routes of impregnating magnetic nanoparticles (MNPs) into PNIPAM hydrogel structures.
2) To develop thermo-magneto-responsive PNIPAM-base composite hydrogels containing MNPs cores with adequate colloidal stability, unabated dual-responsive nature and narrow size distribution by using facile synthetic route.
3) To investigate the adsorption-desorption behaviours and mechanisms of composite hydrogels towards $Cr^{3+}$ ions under the effect of temperature variation.
4) To evaluate the adsorption-desorption mechanisms of composite hydrogel with addition of co-monomer with metal-ions recognizing group

## 1.8 Scopes of Study

At the initial stage of this research work, different routes of encapsulating MNPs with PNIPAM cross-linked polymeric hydrogel matrix were performed in an ultimate quest for the facile way to develop colloidally stable, monodispersed PNIPAM composite hydrogels with definite core-shell structures and well-maintained dual-responsiveness. First and foremost, PNIPAM was directly gelated onto bare MNPs produced from co-precipitation method via one-step free-radical polymerization (FRP) at 70 ºC under stirring for 4 h. Then, another batch of PNIPAM-MNPs composites were produced by two-step route. Bare MNPs were first pre-treated by surface modification with silanization precursor, 3-(trimethoxysilyl)propyl methacrylate (MPS) at 40ºC in alcoholic solvent to impart double-bond vinyl terminal groups (-C=C-) on surface of MNPs to react with *N*-isopropylacylamide (NIPAM) monomers during polymerization. Again, the surface modified MNPs were proceeded to PNIPAM gelation via FRP to form composite hydrogels.

On the other hand, another two batches of PNIPAM-MNPs were developed through pre-coating by silica layer with the several essential aims including; maintaining colloidal stability of MNPs cores during polymerization, enhancing the structural robustness of the MNPs seeds for constituting well-defined core-shell structures and minimizing the cluster size of the enveloped MNPs to avoid undesired self-agglomeration of composite hydrogels driven by magnetic dipole attraction. The silica coating of MNPs was pursued through Stöber process using tetraortho silicate (TEOS) as silica forming precursor. Prior to silica coating, the co-precipitated bare MNPs were pre-functionalized by poly(vinylpyrrolidone) (PVP) to impart steric stabilization on MNPs when dispersed in the basic alcohol-ammonia co-solvent during Stöber process. PVP also functions as bridging agent to facilitate effective coating by forming hydrogen bonds between silanol (-SiOH) groups of silica and surface carbonyls (-C=O) of PVP.

Next, one batch of composite hydrogels were produced by gelating PNIPAM onto silica-coated PVP-MNPs through FRP. Another batch of composite hydrogels were synthesized by post-silanization gelation, in which the silica-PVP-MNPs seeds were pre-modified by silane, MPS to introduce reactive surface vinyl groups before PNIPAM encapsulation via FRP. After that, the physio-chemical properties of all composite hydrogels with different compositions were characterized by using following instrumentations. First, the presence of functional groups and the composition weightages of each passivating layers that constituting composite hydrogels were characterized by fourier transform infrared spectroscopy (FT-IR) and thermal gravimetric analysis (TGA), respectively. Second, the morphology and particle structure were examined by transmission electron microscopy (TEM).

Then, the thermo-responsiveness of the composite hydrogels was perused by applying dynamic light scattering (DLS) equipment to monitor the change in hydrodynamic diameter ($D_h$) of the composite hydrogels and their size distribution as a function of temperature. In the term of magneto-responsiveness, the magnetopheresis and colloidal stability were investigated with and without influence of external magnetic field, respectively, by using UV-vis spectrophotometer to monitor the concentration change of composite hydrogels in aqueous suspensions as a function of time. After all, the PNIPAM-encapsulated MNPs composite hydrogels of core-shell structures having collective superiority in terms of colloidal stability, functional dual-responsiveness and particle distribution were selected as adsorbents for the $Cr^{3+}$ adsorption-desorption performance study.

In the following stage of research works, the chromium (III) ($Cr^{3+}$) cations adsorption abilities of the composite hydrogels were evaluated and the adsorption capacities of hydrogels were obtained under the effects of initial $Cr^{3+}$ concentration, $C_0$ (20 – 80 mg $L^{-1}$) and the dosage of composite hydrogels (0.02 – 0.1 g $L^{-1}$). Next, the adsorption isotherm analyses were performed by fitting the adsorption data to different isotherm models to elucidate the adsorption mechanisms acquired by the composite hydrogels for different temperature. In addition, thermally actuated $Cr^{3+}$ adsorption-desorption fashion of the composite hydrogels was evaluated by carrying out temperature-swing adsorption performance assessments under temperature switching from 298 K to 323 K and reversing back to 298 K. Before magnetic separation, duration of 24 h was allowed for the adsorption system to achieve equilibrium adsorption at each temperature under shaking.

The extent of uptake and release of $Cr^{3+}$ was then delineated by the change in a dimensionless quantity denoted as $q_e$ / $C_e$ at different temperatures throughout the

heating and cooling cycles, where $q_e$ refers to the equilibrium adsorption capacity and $C_e$ represents the equilibrium $Cr^{3+}$ concentration measured for every temperature evaluated. Nonetheless, the magnetic phase separation was a slow process under low-gradient magnetic field, and prolonged duration of magnetic separation could cause certain extent of aggregation induced by magnetic dipole moment which could impair the adsorption-desorption efficiency of the hydrogel systems.

Next, the adsorption kinetics studies were also conducted to the rate of adsorption, adsorption mechanism on adsorption efficiency of the hydrogels. However, the rate of $Cr^{3+}$ adsorption by hydrogels was too fast that the kinetics study was not possible to be performed under the effect of temperature change.

## 1.9 Organization of the Thesis

This thesis comprises of five chapters that covers the introduction, literature review, materials and methodology, results and discussion, while the last chapter refers to conclusions and recommendations which conclude the important findings of this research project. Each chapter of the thesis is summarized and outlined as follow:

Chapter one outlines the research overview of utilizing thermo-magneto-responsive PNIPAM-base composite hydrogels as adsorbents for the perusal of thermo-responsive adsorption-desorption of chromium (III) cations in aqueous solution. Problem statement was highlighted and discussed based on the technical challenges on the synthesis of dual-responsive PNIPAM-MNPs composite hydrogels and the limitations of metal adsorption by the composite hydrogels. It was followed by a list of objectives corresponding to the main scope skeleton of this research project. Then, the organization of the thesis elucidates the highlighted content of each chapter.

Chapter two presents the literature review of various reported research works in this research area. In the beginning section, it encompasses the introduction of major types of stimuli-responsive hydrogels, it is followed by the different synthetic routes and structural designs of the composite hydrogels containing both organic polymeric hydrogel and inorganic nanoparticles. Then, various commonly used existing techniques for the removal of heavy metal ions from wastewater was discussed. In the section of adsorption, myriads of both biopolymeric and synthetic polymeric hydrogels applied for metal ion removal was outlined into concise and brief descriptions. At the end of this chapter, literatures on application of thermo-responsiveness of PNIPAM-base hydrogels for thermal actuated adsorption and desorption of metal ions was presented.

Chapter three elaborates the experimental materials and methodology. The laboratory-scale procedure of synthesizing PNIPAM-encapsulated MNPs composite hydrogels and characterization processes upon physio-chemical properties including the morphological analyses, thermo-responsiveness, colloidal stability and magnetophoresis of the produced composite hydrogels were outlined. The detailed overview of the experimental work flow was summarized in a flowchart. Then, the procedures of adsorption-desorption performance studies, the equipment used, adsorption isotherm models and adsorption kinetic studies were also described in the subsequent section. Last but not least, the required equations for all data analyses were also provided in the same chapter.

Chapter four summarizes all the experimental results that include the characterization on physio-chemical properties of composite hydrogels, and the adsorption-desorption analyses. The characterization section consists of functional groups identification, morphological analysis, temperature-swing thermo-responsive

behaviour, investigations on colloidal stability and magnetophoresis with their respective explanation. The adsorption-desorption performance section refers to the equilibrium adsorption tests, adsorption isotherm analyses, temperature-swing adsorption-desorption test and adsorption kinetics analyses.

Lastly, chapter five embraces the conclusions for the important findings and several recommendations proposed for the future research.

# CHAPTER TWO

# LITERATURE REVIEW

This chapter highlights the important review of the published works that are critically relevant to this research. The current development of nano-structures especially stimuli-responsive composite nano-structures and their applications in heavy metal adsorption have been summarized in the following sections. First and foremost, the discussion on various types of stimuli-responsive polymeric hydrogels and their responses reflected in physio-chemical property change under influence of external stimuli effect was included in the initial section. In the next section, different synthetic routes and structural designs of thermo-responsive PNIPAM-base composite hydrogels were discussed. It is followed by the brief introduction of different commonly employed techniques for heavy metal removal. Meanwhile, under the section of adsorption, elaborations and reviews on reported application of myriad hydrogel types for metal ion adsorption and recovery. Subsequently, thermal actuated recovery of metal ions and regeneration of thermo-responsive PNIPAM-base hydrogels were elaborated. Lastly, the research gap was highlighted.

## 2.1 Stimuli-responsive Polymeric Hydrogels

Polymeric hydrogels are defined as a type of water-soluble (hydrophilic) cross-linked globular polymeric matrix. Each of these hydrogel particles composed of polymer chains that are cross-linked into a globular gel network structure. The hydrogel matrix with three-dimensional globular conformation is solvated into swollen state in aqueous medium. Its ability to absorb high amount of water is ascribed to the hydrophilic functionalities contained within the hydrogel network such as carboxylates (-COO-), hydroxyls (-OH), amides (-CONH) and so forth that are adhered along the

polymer backbone chains or present as lateral chains across the hydrogel matrix through hydration effect (Ballauff and Lu, 2007).

By and large, the cross-linked hydrogel matrices possess stimuli-responsive properties wherein their hydrophilic functionalities could render a reversible switch in their hydration properties from hydrophilic in nature to being hydrophobic in response to the changes and inductive effects promoted by specific stimuli in surrounding environment. Stimuli includes solution pH, temperature, light as well as electric field. The switch in hydrophilicity of the cross-linked polymer chains that form the hydrogel, leads to conformational change in coil-to-globule manner contributing to the swelling and shrinking mechanism of the entire cross-linked hydrogel network as triggered by the corresponding stimulus. Hence, their tendency to swell and to shrink under the influence of external stimuli makes them to be coined as “smart” or “intelligent” polymeric gels engendering their potential feasibility to be used as ideal materials in various applications for the controlled uptake and release of chemical substances (Gil and Hudson, 2004, Liu and Urban, 2010).

The stimuli that trigger the conformational changes on these smart hydrogels can be classified into three main categories, spanning from physical stimuli such as temperature, light and pressure, chemical stimuli including solution pH and ionic strength to biological stimuli that embraces enzymes (proteins) and other organic substances as illustrated in Figure 2.1. In literatures, most of these classes of stimuli-responsive hydrogels have largely been applied in the studies of biomedical engineering disciplines that embrace tissue engineering and drug delivery. For instance, pressure-responsive hydrogels exhibit decreased viscosity with increasing external shear force. The hydrogels with reduced viscosity can flow in the body fluid system under the applied external pressure force. This allows them to be a potential candidate

for injectable drug delivery system for controlled release of drug within human body fluid (Koetting et al., 2015, Guvendiren et al., 2012, Aulisa et al., 2009). Protein-responsive hydrogels, on the other hand, are usually synthesized by using DNA or other nucleic acids as cross-linking agents that possess functional groups to respond towards signaling molecules including specific enzymes. The incorporation of living cells in these hydrogels allows the detection of the cell proliferation through the penetration of nutrients into the hydrogel network interior (Sood et al., 2014, Xue et al., 2017).

Nonetheless, in the applications of wastewater remediation, only thermo-responsive, pH-responsive and photo-responsive hydrogels have been reported, particularly for the heavy metal ion removal. This is mainly because the temperature, pH and light are the most common factors that can be used as manipulating factors for the removal of heavy metal ions in wastewater (Koetting et al., 2015, Medeiros et al., 2011).

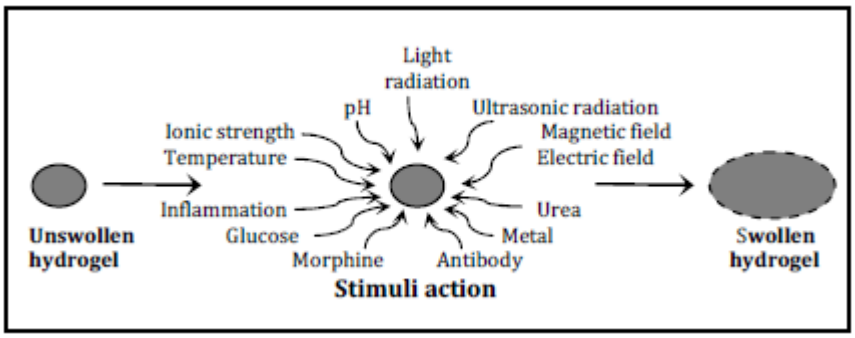


**Figure 2.1**: Schematic illustration of the swelling-shrinking behaviour of stimuli-responsive hydrogels (Nanjundswamy et al., 2009).

### 2.1.1 Thermo-responsive Hydrogels

Thermo-responsive hydrogels are a type of stimuli-responsive polymeric hydrogels which has been extensively studied in line with the recent researches

regarding smart polymeric materials with prominent properties. It has a matrix comprising thermos-responsive polymer chains that are cross-linked into a usually globular conformation. Each of these polymer chains has an ability to undergo transition from extended coil chain to a globular form when temperature rises above its lower critical solution temperature (LCST). Hence, the hydrogel with cross-linked network exhibits conformational change in response to the variation of temperature. The alteration in their matrix structures is reflected as swollen and shrunken states with respect to the temperature change (Medeiros et al., 2011).

At temperature below its LCST, the hydrogel network is hydrated by water molecules imbibed within the matrix. Water is bound by the hydrophilic functionalities causing expansion in network size which results in a swollen hydrogel matrix. On the other hand, as temperature rises above LCST, water-associated hydrogen bonds are gradually broken leading to successive expulsion of water molecules from interior of hydrogel network at increasing temperature until it is fully dehydrated. Hydrophilic functional groups of the hydrogel are invaginated into the interior of the network forming inner hydrogen bonds. By contrast, the hydrophobic ones are instead exposed to the bulk solution which induces phase separation of the hydrogel solid phase from the aqueous bulk. As a result, the dehydration of hydrogel network is portrayed as shrunken matrix. However, the swelling and shrinking behaviour is somehow reversible upon swinging temperature variation across its LCST (Dimitrov et al., 2007).

Numerous kinds of temperature-sensitive polymers have been perused previously and reported in literature. By and large, these thermos-responsive polymers consist of amphiphilic acrylamide ($C_2H_4CONH$) moiety in which its hydrophilic amide portion is hydrated to dissolve as homogenous phase with the bulk solution at temperature below its corresponding LCST, where it is dehydrated into coil form at

above LCST as demonstrated in Figure 2.2. Other temperature-sensitive polymers also comprise of ring-structure pyrrolidine ($C_3H_8NH$) or piperidine ($C_4H_{10}NH$) moiety that contains hydrophilic amine groups as the thermo-responsive part. Table 2.1 outlines different thermo-responsive polymers and their corresponding LCST or phase transition temperature.

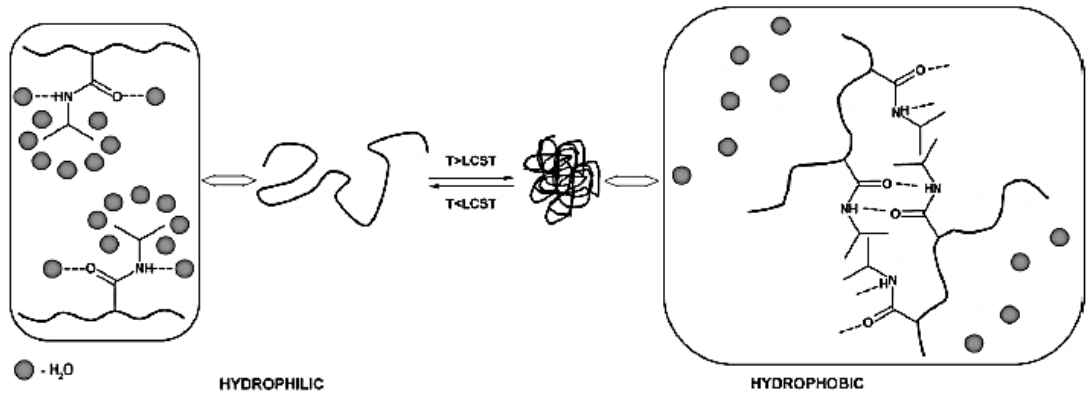


**Figure 2.2**: Schematic illustration of the thermos-responsive phase transition of acrylamide-base polymer (Dimitrov et al., 2007).

**Table 2.1**: Lower critical solution temperature (LCST) of different thermo-responsive polymers (Medeiros et al., 2011, Liu et al., 2009, Kawaguchi, 1999).

| Thermo-responsive Hydrogels | Abbreviation | LCST (°C) |
|---|---|---|
| Poly(*N*-ethylacrylamide) | PNEAM | 72 |
| Poly(*N*-cyclopropymethacrylamide) | PNCPMAM | 59 |
| Poly(*N*-methyl-*N*-ethylacrylamide) | PNMNEAM | 56 |
| Poly(*N*-acryloylpyrrolidine) | PNAOP | 56 |
| Poly(*N*-ethylmethacrylamide) | PNEMAM | 50 |
| Poly(*N*-cyclopropylacrylamide) | PNCPAM | 45.5 |
| Poly(*N*-isopropylmethacrylamide) | PNIPMAM | 44 |
| Poly(*N*-methyl-*N*-isopropylacrylamide) | PNMNIPAM | 22.3 |
| Poly(*N*-n-propylacrylamide) | PNNPAM | 21.5 |
| Poly(*N*-methyl-*N*-*n*-propylacrylamide) | PNMNNPAM | 19.8 |
| Poly(*N*-acryloylpiperidine) | PNAOP | 5.5 |

Amidst a plethora of thermo-responsive polymers, poly(*N*-isopropylacrylamide) (PNIPAM) has emerged as the most perused candidate, mainly attributed to its near-room-temperature LCST at around 32 °C. It upstages other

polymers of this kind to be a promising polymer for cross-linked hydrogel formation. Moreover, PNIPAM hydrogel is known to have the fastest and greatest extent of thermo-responsive VPT compared to other hydrogels of this type which exhibits 50-fold of volume change within around 1 μs as reported by Wu and co-workers (2018). It is always regarded that its outstanding thermos-responsive property has been profoundly prominent for extensive applications (Wu et al., 2018, Medeiros et al., 2011, Oh and Park, 2011).

The thermo-responsive VPT of PNIPAM hydrogel in water is schematically portrayed in Figure 2.3. The hydrogel is swollen at its initial state at temperature below its LCST. As temperature is increased above the LCST, the shrinking mechanism is driven by dehydration which in turn arises from the entropic gain as water-linked hydrogen bonds are dissociated and water molecules are expelled from the hydrogel network.

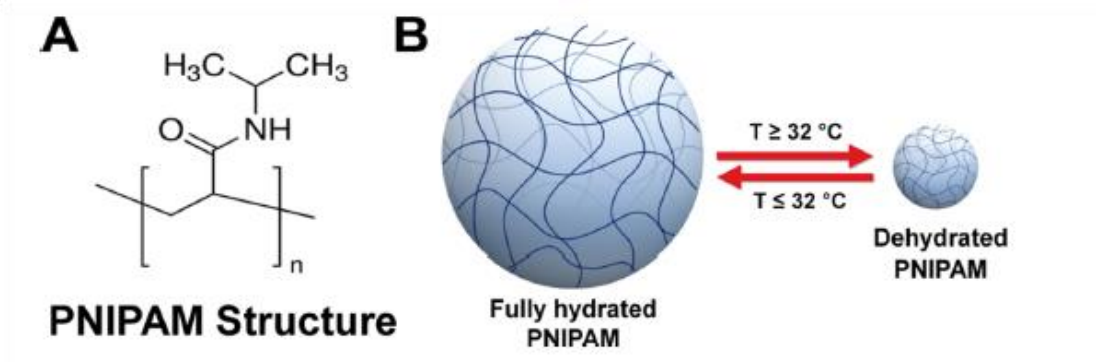


**Figure 2.3**: A) Chemical structure of poly(*N*-isopropylacrylamide) (PNIPAM); B) schematic illustration of the volume phase transition of cross-linked PNIPAM hydrogel (Wu et al., 2018).